Multifractal Analysis of Line-Source Plume Concentration Fluctuations in Surface-Layer Flows

D. FINN AND B. LAMB

Laboratory for Atmospheric Research, Washington State University, Pullman, Washington

M. Y. LECLERC

Laboratory for Environmental Physics, University of Georgia, Griffin, Georgia

S. LOVEJOY AND S. PECKNOLD

Physics Department, McGill University, Montreal, Quebec, Canada

D. SCHERTZER

Laboratoire de Modelisation en Mecanique, Université Pierre et Marie Curie, Paris, France

(Manuscript received 22 July 1999, in final form 8 April 2000)

ABSTRACT

A codimension multifractal methodology was used to analyze and to model scalar concentration fluctuations within sulfur hexafluoride tracer gas plumes from a line source in atmospheric surface-layer flows. Correspondence was exhibited between the double trace moments parameters α and C_1 of the codimension methodology and the experimentally measured plume concentration characteristics of peak-to-mean ratio and concentration fluctuation intensity. Data series were generated using an extremal Levy, stochastic multifractal model, with the experimental α and C_1 as inputs. Uncertainties in experimentally determined plume characteristic values overlapped the uncertainties in model-simulated values. The utility of the procedure includes 1) characterizing the state of scalar turbulent mixing, 2) helping to evaluate and to model hazardous plume concentrations, and 3) being able to estimate the probability of realizing extreme events at timescales of observation beyond or at magnitudes in excess of those present in the actual observations.

1. Introduction

Turbulent mixing of a contaminant plume in the atmosphere produces an extremely complicated pattern of contaminant concentration. Scalar (contaminant)-rich eddies are stretched and distended by the action of turbulent motions while scalar-poor fluid is entrained into the plume along similarly deformed eddy structures. The resulting concentration time/space field is highly irregular, reflecting the disparities in concentration between juxtaposed eddies. For a time series at a fixed location, the concentration record can exhibit extreme intermittency, rapid changes, and the occurrence of relatively rare but large events when peak concentrations are recorded.

An understanding of plume behavior and scalar mixing in varying conditions is necessary for developing appropriate emergency response plans in the event of the inadvertent airborne release of toxic or other hazardous substances. The concentration time series observed at a receptor site will depend on the magnitude of the release as well as factors such as the size and geometry of the source, the source-to-receptor (streamwise) distance, the location of the receptor with respect to the centerline of the mean plume axis, topographic effects, micrometeorological variables such as variations in wind speed and direction, and atmospheric stability.

The measurement and modeling of point-source plume behavior and the natural stochastic variability associated with it have been extensively studied (e.g., Ramsdell and Hinds 1971; Hanna 1984; Larsen and Gryning 1986; Mikkelsen et al. 1987; Hanna and Insley 1989; Sawford and Stapountzis 1986; Stapountzis et al. 1986; Yee et al. 1993, 1994; Peterson and Lamb 1992, 1995; Peterson et al. 1990). Commonly used descrip-

Corresponding author address: Dennis Finn, Washington State University, Dept. of Civil and Environmental Engineering, Sloan 101, Pullman, WA 99164-2910.
E-mail: dfinn@mail.wsu.edu

© 2001 American Meteorological Society

tions of concentration exposure at a receptor site in the atmosphere are the mean concentration $\overline{c}$, the standard deviation σ_c, the concentration fluctuation intensity i_c ($i_c = \sigma_c/\overline{c}$), the intermittency factor (the fraction of time a receptor is within the plume), and the peak-to-mean concentration ratio ($P/M = c_{\max}/\overline{c}$), where $c_{\max}$ is the 99th-percentile concentration.

Most traditional approaches for modeling and predicting plume behavior use some variant of a Gaussian plume model with empirical parameterizations of the wind field. Alternative methods for modeling plume concentration fluctuations include the use of Lagrangian models (Sawford 1985; Peterson et al. 1995) and large eddy simulation (Shen and Leclerc 1994). Existing models commonly produce results that are within a factor of 2 of measurements. The mean concentration and P/M are the most essential variables for evaluating the maximum potential hazard stemming from an inadvertent plume release. Knowledge of the mean concentration is an indication of the total mass of hazardous material, and P/M is important if short-term peak values are much more dangerous than the mean concentration. Models for internal plume concentration fluctuations can be useful for evaluating hazards if they can be linked to a model describing whether a receptor is in or out of a plume (i.e., point-source plume meander). The purpose of this paper is to describe an alternative multifractal model for predicting scalar mixing, concentration fluctuation, and P/M within atmospheric plumes, both within better-mixed portions of the plume and in the poorly mixed volume of the plume along the margins.

Because of the scale invariance of the underlying dynamical process, it is natural to apply scaling techniques to the study of plume behavior and scalar mixing. These processes have been studied by applying traditional monofractal box-counting techniques to multifractal fields (e.g., Sreenivasan et al. 1989; Sreenivasan 1991; Constantin et al. 1991; Muzzio et al. 1992; Malinowski and Leclerc 1994; Sykes et al. 1995; Praskovsky et al. 1996). Rather than approximate the concentration by a geometrical set of points, the multifractal approach allows for a hierarchy of different concentration events, each with its own degree of sparseness. A basic description of multifractal theory and the distinctions between the traditional and codimension approaches is found in the appendix.

The results presented here are based upon an extensive set of sulfur hexafluoride (SF_6) tracer gas measurements downwind from a line source. The experiment from which the data were obtained is described, and some of the limitations on the use of the dataset with respect to multifractal analysis are discussed. The methodology used in the multifractal analysis is then summarized. This summary includes a description of a stochastic multifractal model. The results section describes the determination of a set of parameters from the multifractal analysis of the experimentally measured SF_6 time series. These parameters were then utilized in the stochastic multifractal model that was used to generate output for comparison with the measured experimental data. The consequences and possible applications of this approach are then discussed.

2. Experimental summary

A field study, originally designed to evaluate flux footprint models, was conducted during June 1992 on the Hanford diffusion grid near Richland, Washington. Details of this study can be found in Finn et al. (1996). The site is located in a 40-km basin on gently sloping terrain at an elevation of approximately 200 m above sea level. An open canopy of sagebrush 1–1.5 m high is the dominant vegetation, with a zero plane displacement d of 0.75 m and roughness length z_0 of 0.14 m.

A 400-m line source of SF_6 passive scalar tracer gas was deployed at canopy height (1.0 m) approximately perpendicular to the prevailing wind direction. The line source was approximated by point sources spaced 4 m apart along the 400-m length. Four 10-m towers were located at downwind distances x of 50, 100, 175, and 250 m along a line normal to the line source. Each tower was equipped with a 3D sonic anemometer and a fast-response SF_6 analyzer (Benner and Lamb 1985) with a 30-ppt detection limit and 1/e response time of about 1 Hz. Manual calibrations were completed before and after each tracer release period. Zero and span checks were conducted with an automated system at each instrument, generally every 30 min.

Tracer was released continuously at a steady rate when winds were across the line source and parallel to the tower array. Releases and observations were made over a wide range of atmospheric stabilities. Measurements were made at a measurement height of $z_m = 10$ m during the first phase of the experiment and 5 m during the second. Data were recorded continuously at either 10 or 20 Hz from both the anemometers and tracer analyzers.

An important point with regard to the experimental configuration and the basis of the multifractal methodology used in the analysis is that the theoretical basis of the multifractal methodology assumes statistical translational invariance of the field being measured. Although this approximation may be good for atmospheric turbulence, the SF_6 scalar statistics depend strongly on the measurement location with respect to the source. The measured signal is not statistically translationally invariant in space given the spatially localized nature of the line source. The inhomogeneity in the SF_6 tends to become more exaggerated close to the line source and decreases downwind with the increase in plume size and mixing. When the SF_6 sensor is fully embedded in the plume, the field approaches a more homogeneous condition. However, when the sensor is near the margin of the plume with respect to the vertical plume centerline, the field is highly inhomogeneous. In fact, the sensor can lie either in or out of the plume.

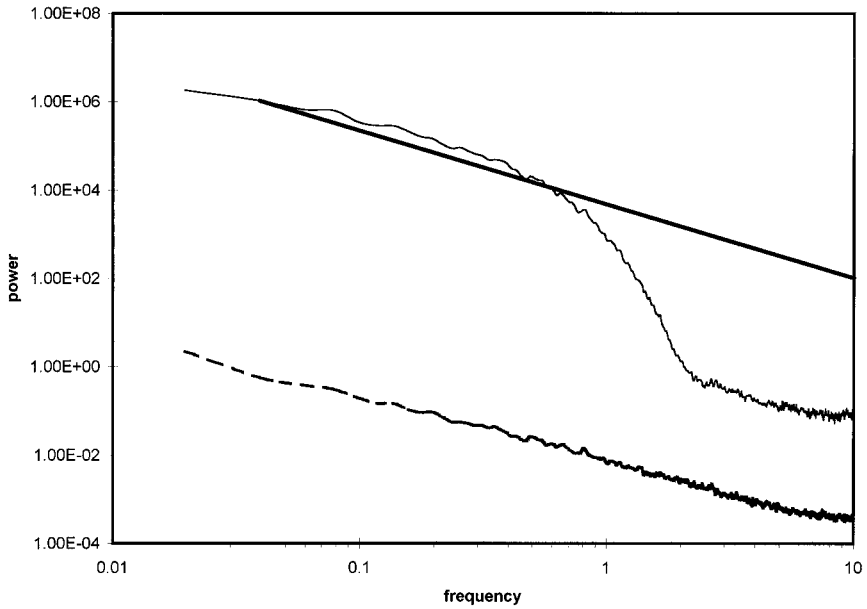

FIG. 1. SF_6 Fourier power spectrum (thin solid line) for the 175-m tower on yeardays 173 to 174, 2300–0100 local time. The bold solid line represents a $-5/3$ slope; the bold dashed line is the temperature spectrum for the 175-m tower.

Whether the sensor lies in or out of the plume depends on the stability conditions in the atmosphere. In stable conditions, vertical plume spread is inhibited, and the plume sometimes fails to rise to the height of the sensors, particularly at the 50- or 100-m towers. In unstable conditions, the SF_6 signal can be affected by strong downdrafts of clean SF_6-free air from aloft that will have the effect of introducing zeros into the data record. Increasing the time and/or distance available for plume spread and mixing will increase the statistical homogeneity of the plume and reduce the chances for the sensor encountering large parcels of SF_6-free air. A simple model of this effect is that the measured signal represents a mixed monofractal (zeros, clean air) and multifractal turbulent (plume) process.

The key point is that the multifractal results are primarily sensitive to the state of mixing in the plume, which, in turn, depends upon the position of the receptor within the plume, distance from the source, and turbulence regime. Assuming power-law scaling exists for the measurements, the multifractal technique can be used to model plume mixing conditions with respect to these factors.

3. Summary of methodology

a. Introduction

Because of the existence of stable (attractive) multifractal processes, it is natural to postulate that the basic multifractal exponent functions are described by three universal parameters, α, C_1, and H (Schertzer et al. 1995; Schertzer and Lovejoy 1993, 1997). The multifractal codimension methodology that will be used to estimate the parameters α, C_1, and H from an experimental signal is the double trace moments (DTM) algorithm (Schertzer and Lovejoy 1993; Tessier et al. 1994; Lavallee et al. 1993). Examples of its exploitation and related multifractal studies can be found in Tessier et al. (1994), Schmitt et al. (1992, 1993, 1995, 1996), Chigirinskaya et al. (1994), Salvadori et al. (1994), Pandey et al. (1998), and Schertzer and Lovejoy (1993). The theoretical development of the codimension formalism has been described in Schertzer and Lovejoy (1987, 1989, 1991, 1993), Wilson et al. (1991), and Lavallee et al. (1993).

Successful application of the method depends on the presence of power-law scaling. The first step in the procedure is to confirm the presence of power-law scaling and identify the frequencies bounding the scaling range. Optimum estimates of α and C_1 are made using the longest possible linear power-law scaling range of the inertial subrange in a Fourier power spectrum (Fig. 1). An inner, high-frequency scaling break f_i and an outer, low-frequency scaling break f_o can be seen bounding a power-law inertial subrange in the example SF_6 power spectra. The original data series is then block averaged, replacing the original by a modified data series in which the highest frequency present will equal f_i. The individual values in this modified, highest-available-resolution data series are denoted ρ.

The inner scaling break is generally determined by the resolution of the measurement system because the inner scale of the phenomenon is the very small dissipation scale. The scaling break f_i is, therefore, de-

pendent on the resolution of the SF_6 measurement system and the physical limitations of the instrumentation. Attaching any physical significance to the scaling observed in the SF_6 spectra in Fig. 1 at frequencies greater than 2 Hz is suspect, because those frequencies are beyond the resolution of the SF_6 analyzers.

The data series ρ must then be transformed into a ''conserved'' signal before it can be processed in the DTM algorithm. Conservation here refers to the scale-by-scale conservation of the underlying multifractal process. In the context of the current discussion of passive scalar concentrations in the atmosphere, the conserved quantity being passed from larger to smaller eddies in the cascade is the flux of scalar variance. From the expression $\Delta\rho_\lambda = \phi_\lambda^{1/3}\lambda^{-1/3}$ (appendix), the observed, nonconserved concentration time series $\Delta\rho_{\lambda,\mathrm{SF6}}$ is related to the conserved flux $\phi_{\Lambda,\mathrm{SF6}}$, all implicitly nondimensional with normalization. The transformation is accomplished through the scaling factor of the form λ^{-H}. The notation λ represents the scale of resolution. The parameter H is one of three universal multifractal parameters and characterizes the degree of nonconservation.

In general, a measured signal ρ is not conserved (e.g., a concentration time series) and is dependent on the scale of observation of a process (i.e., the resolution of the measurements or averaging time of the measurements). When H is known, a conserved data series can be obtained from ρ by filtering in Fourier space by dividing by $|f|^H$, where f is frequency. Values of H less than 0 represent fractional differentiation, and H greater than 0 represents fractional integration. A forward transform is performed on the time series, the Fourier components are divided by $|f|^H$, the result is inverse transformed back to real space, and the absolute values of the result are taken. An alternative for a one-dimensional time series, approximately equivalent to fractional differentiation by order 1, is replacing the block-averaged time series by the absolute differences between adjacent data points ρ.

For a specific measured process, H is not necessarily known ahead of time, and the alternative data transform is used. It can be determined from experimental data using

$$H = \frac{\beta - 1 + K(2, 1)}{2};$$

$$K(2, 1) = \frac{C_1(2^\alpha - 2)}{\alpha - 1}, \tag{1}$$

where β is the absolute value of the slope in the inertial subrange of a power spectrum for an observed process (e.g., $\beta = 5/3$ for the energy flux ε), and α and C_1 are determined using the DTM algorithm.

To illustrate better the procedure leading to the calculation of the double trace moments and the use of λ, begin with Fig. 1. Observe the scaling range for SF_6 extending from $f_i \approx 0.5$ Hz to $f_o \approx 0.05$ Hz. There are 36 000 points for a 0.5-h record sampled at 20 Hz. Recall that the highest resolvable frequency is $1/(2\Delta)$, where Δ is the sampling interval. Block averaging the time series at 20 points per block results in a time series ρ_{SF6} with 1800 points in which the highest resolvable frequency is f_i. A conserved time series ϕ_{SF6} is then obtained by taking the absolute differences between adjacent block-averaged data points. The lowest frequency obtainable from a given data series is given by $1/(N\Delta)$, with N being the number of points. The conserved time series is split into subrecords A of length N such that the lowest frequency present in the subrecords is approximately equal to f_o. In the current case, 20 points would give a frequency of 0.05 Hz. The subrecord length A would thus be 16 or 32 points, in powers of 2, yielding 112 or 56 subrecords, respectively, per 0.5 h.

The parameter λ is a scale ratio equal to the largest scale of significance, for example, the length of the time/space series or outer scale of the turbulence, divided by the resolution of series. The largest scale ratio is denoted Λ and equals 16 or 32 in the current example. The value of λ can be adjusted by varying the scale of resolution between the highest resolution Λ (smallest scale) and resolutions intermediate to the largest scale such that $\Lambda \geq \lambda \geq 1$.

The statistical moment scaling function $K(q, \eta)$ is defined from

$$[(\phi_\lambda^\eta)_\lambda^q] \cong \lambda^{K(q,\eta)}, \tag{2}$$

where q and η are the orders of the statistical moments. For conserved universal multifractals, $H = 0$ and the exponent $K(q, \eta)$ is

$$K(q, \eta) = \begin{cases} \eta^\alpha \dfrac{C_1}{\alpha - 1}(q^\alpha - q) & \alpha \neq 1 \\ C_1 \eta q \log(q) & \alpha = 1, \end{cases} \tag{3}$$

where the multifractal parameter α is the index for Levy distributions, which describe stable, generally non-Gaussian random cascade generators (Feller 1971; Wilson et al. 1991; Schertzer and Lovejoy 1991, 1993) and can serve as a multifractal index. It is constrained by $0 \leq \alpha \leq 2$. The index $\alpha = 2$ describes a multifractal process with an approximately lognormal probability distribution. As the value of α decreases from 2, the corresponding signal becomes increasingly intermittent, with very large fluctuations and increasing P/M ratio. From Eq. (3) and the general relation $K(q, \eta) = K(q\eta, 1) - qK(\eta, 1)$, we obtain for $\alpha \neq 1$

$$K(q, \eta) = \eta^\alpha K(q, 1). \tag{4}$$

The third universal parameter, C_1, is the codimension of the mean process or measured signal and characterizes its inhomogeneity. Its value will increase in response to sparse and intermittent or highly fluctuating and variable signals and will decrease for a more uniform signal. A value of $C_1 = 0$ implies that the mean

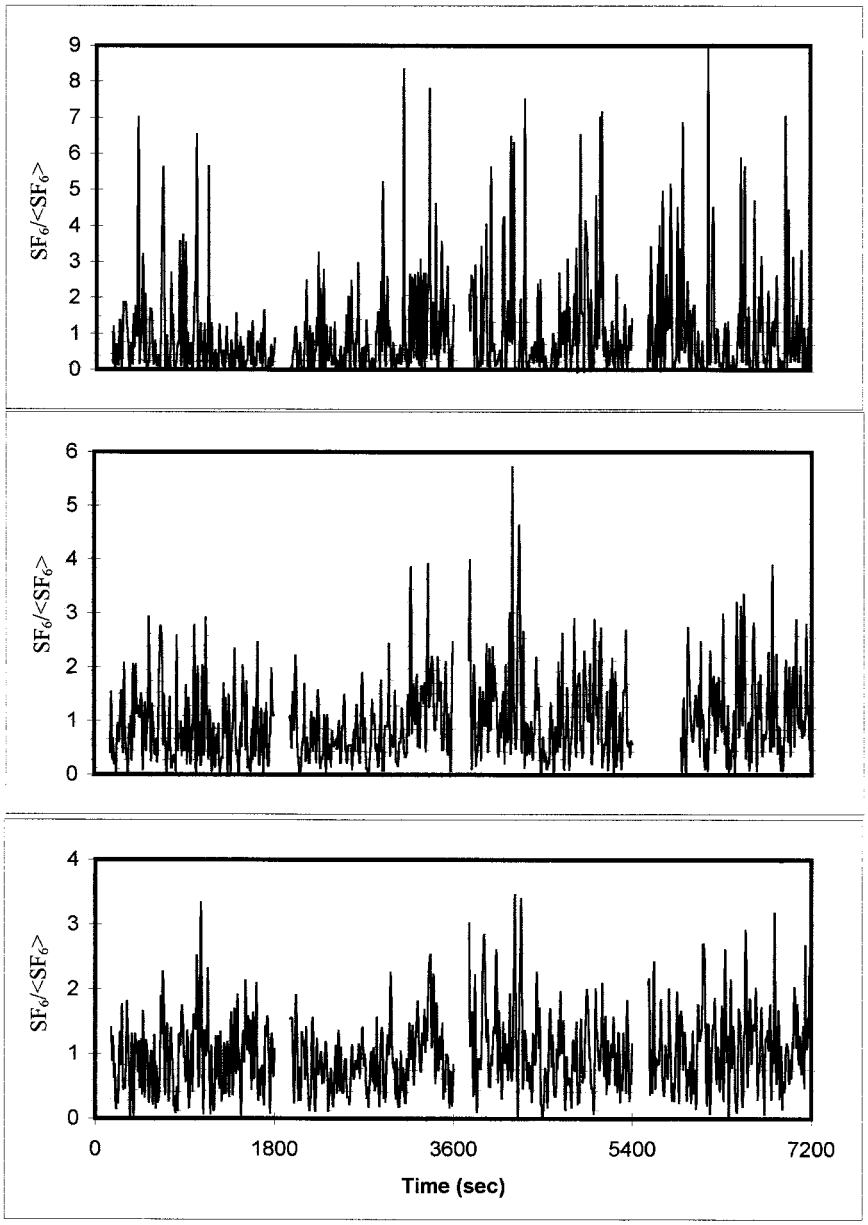

FIG. 2. Normalized SF_6 concentration time series ($SF_6/\langle SF_6\rangle$) for the 50-, 100-, and 175-m towers, respectively, from top to bottom on yeardays 173 to 174, 2300–0100 local time, averaged to 0.1 Hz. Gaps in the records represent calibration periods.

is space filling (complete homogenization of the conserved process).

b. Estimation of α, C_1, and H from experimental data

For the purpose of illustration, the procedure is demonstrated using example SF_6 time series from the experiment. Three concurrent 2-h time series at the 50-, 100-, and 175-m towers, in weakly to moderately stable conditions, are shown in Fig. 2 (nondimensional scaling parameter $z/L = 0.05$, yeardays 173–174, 2300 to 0100 local time, where $z = z_m - d$, and L is the Obukhov length). These examples represent 20-Hz time series averaged to 0.1 Hz. Note the distinctions in character between the time series. The 50-m time series exhibits greater intermittency and relatively larger fluctuations above its mean than do the 100- and 175-m time series.

Implementation of DTM begins with the highest-resolution data series ϕ_Λ. The double trace moments Tr are defined as

$$\mathrm{Tr}_\lambda(\phi_\Lambda^\eta)^q = \left\langle \sum_A \left(\int_{B_\lambda} \phi_\Lambda^\eta \, d^D x \right)^q \right\rangle \propto \lambda^{K(q,\eta)-(q-1)D}, \quad (5)$$

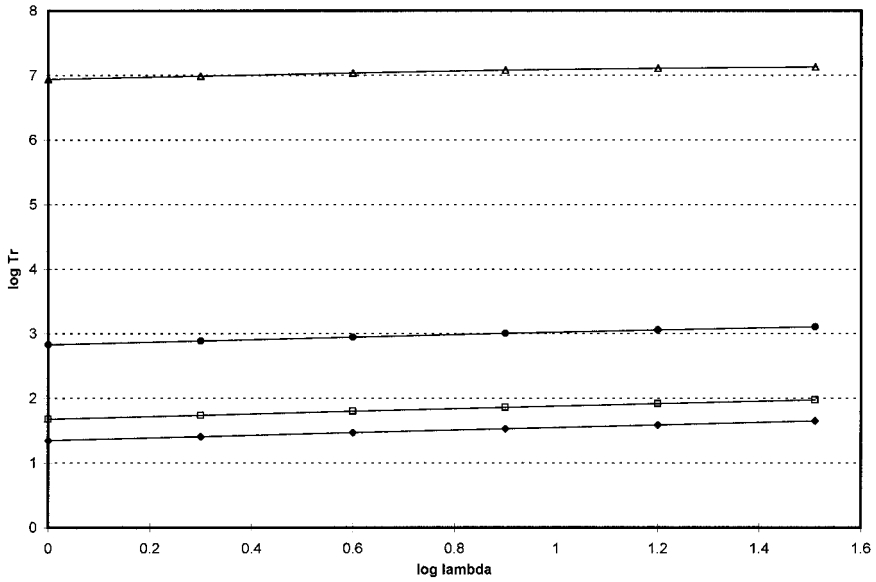

FIG. 3. Plot of the double trace moments logTr vs logλ showing selected values of η for $q = 0.8$ and record length of 2^5 for the 175-m tower, yeardays 173 to 174, 2300–0100 local time (◆: $\log\eta = -1$, □: $\log\eta = -0.5$, ●: $\log\eta = 0$, △: $\log\eta = 0.5$). The slopes yield estimates of $K(q, \eta)$.

where q and η are the orders of the statistical moments. The D represents the dimension of the sampling, equal to 1 for a time series. Individual data points in the conserved time/space series ϕ, at the inner, highest-resolved scale Λ, are raised to the power η. The scale resolution λ is degraded in successive steps from the highest resolution $\lambda = \Lambda$, equal in length to A, to $\lambda = 1$ for each scaling subrecord A. This degradation is done using disjoint subsets B covering the subrecords A. These subsets are usually some power of 2 in length and are given by Λ/λ. The result for each B is raised to the qth power. The $\langle\ \rangle$ denotes ensemble averaging over the available number of subrecords A at each λ. The results reported below are based on $q = 0.8$ for reasons discussed later; the values of η ranged from 0.1 to 10 in 0.1 $\log_{10}$ increments (i.e., $[-1, 1]$). Estimates of Tr can be obtained by ignoring the $D(q - 1)$ factor in the exponent [i.e., Eq. (2)].

Plotting log(Tr) versus logλ yields a set of slopes, one for each value of η, that are used to obtain estimates of $K(q, \eta)$ (Fig. 3). The changes in slope between η can be subtle and were determined by linear regression. An estimate for the parameter α is then found from the slope given by plotting $\log|K(q, \eta)|$ versus $\log\eta$ using Eq. (4) (Fig. 4). The break in linearity for low values of η is related to measurement noise and sensor resolution. The break in linearity for high values of η is related to divergence and/or sample size limitations, which are discussed below. Parameter C_1 is obtained using Eq. (3) and the fact that $K(q, \eta) = K(q)$ for $\eta = 1$. The linear range should include $\eta = 1$ for C_1 to be estimated reliably. Last, H is obtained from Eq. (1).

To achieve as unambiguous an evaluation of the approach as possible for a certain set of plume mixing conditions, 2-h data records were used during which the flow field was judged to be quasi-stationary. Quasi-stationary conditions were commonly realized, primarily due to drainage flows, but also during the passage of some synoptic fronts. The 2-h record block was chosen because it represented the approximate maximum length for which quasi-stationary conditions could be realized for any appreciable number of cases. Quasi-stationarity was desirable to obtain multifractal parameter estimates representative of certain scalar mixing conditions by using the most reliable possible estimates of the scaling range and β. In general, the 2-h data records were split into four separate 0.5-h subrecords to eliminate spurious spectral scaling from interruptions in the ambient signal during span periods. The cases used included representatives from each of the four towers.

c. Stochastic modeling

The parameters α, C_1, and H can be used as the inputs into stochastic models that generate Levy variables and multifractal fields. These models are useful for studying in-plume mixing and improving the ability to estimate the potential for hazardous extreme values that might not be well represented in a limited experimental dataset. Numerical implementation of continuous (in scale) multifractal processes are described in Wilson et al. (1991), Pecknold (1993), and Tchiguirinskaia et al. (2000).

Briefly, ''extremal'' Levy variables are generated from a uniform $U \sim (0, 1)$ distribution using the appropriate values of α and C_1. Extremal Levy probability distributions decay exponentially for positive values $[\Pr(>y) \sim \exp(-|y|^{\alpha'})]$ but only decay according to a

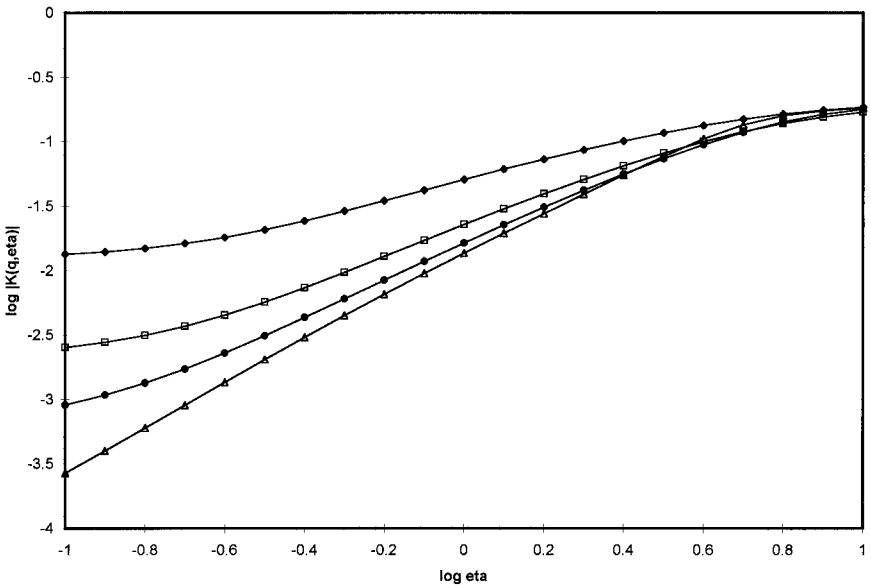

FIG. 4. Plot of the DTM $\log|K(q, \eta)|$ vs $\log\eta$ for $q = 0.8$ and record length of 2^5 for the 50- (♦), 100- (□), 175- (●), and 250-m (△) towers on yeardays 173 to 174, 2300–0100 local time. The slopes in the scaling range yield estimates of α. Note the increase in slope as the distance increases.

power law for negative values [$\Pr(>y) \sim |y|^{-\alpha}$] where $1/\alpha + 1/\alpha' = 1$ and y are thresholds at which each probability Pr is calculated. This Levy noise is normalized using factors that contain α and C_1 and is fractionally integrated by Fourier filtering to yield a $1/f$ noise. The result is exponentiated and passed into a Fourier filter where it is fractionally integrated by $|k|^{-H}$, where k is the wavenumber. The fractional integration only affects the components with the modulus of the wavevector $|\mathbf{k}| > 0$; therefore, the mean must be fractionally integrated in real space or frequent negative values will result.

To adjust approximately the mean ($|\mathbf{k}| = 0$, the zero Fourier component), all model values were adjusted upward by the magnitude of the largest negative value (i.e., a constant was added), returning a nonzero mean and zero minimum. The resulting time series is a modeled representation of the time series from which α, C_1, and H were determined. For $\alpha \leq 1$, the stochastic results are undefined. An example model data series representative of a well-mixed, homogeneous field is shown in Fig. 5.

4. Results

a. Fourier analysis

The first step was to determine the power spectra, scaling ranges, and β for each of the 2-h data records. Using the maximum range possible, typically about one decade, the determination of the experimental values of β for SF_6 ranged from 1.23 to 1.94 with a mean of 1.61.

Previous studies (Kaimal et al. 1972) have shown that the low-frequency scaling break f_o is a function of atmospheric stability and measurement height. For the SF_6 plumes, however, f_o is also considerably influenced by the lack of statistical translational invariance discussed in the experimental section. Thus the scaling range, the difference between the two breaks, is limited by the lack of homogeneity and sensor limitations. Most of the individual analyses used subrecord lengths A of 16 or 32 block-averaged data points.

An expression of the inhomogeneity in the SF_6 plume is illustrated in Fig. 1. The temperature spectrum, representing a more truly homogeneous field, scales to lower frequencies than does SF_6. For temperature, a more complete range of eddy-motion sizes and frequencies are involved with dispersion on the scale of the experiment. In contrast, the low-frequency scaling break for SF_6 occurs at a higher frequency because the larger, lower-frequency atmospheric motions are expressed in the SF_6 record as zeros with the consequence of loss of power in the Fourier spectrum. For sufficiently advanced plume spread and mixing, the SF_6 field would become increasingly homogeneous and the scaling range would increase.

b. Determination of α, C_1, and H for SF_6 experimental data

Equation (5) was applied to the maximum number of available scaling subrecords for each 2-h data record as dictated by the Fourier analysis of each test case. The transformation to a conserved signal was accomplished by replacing the block-averaged time series by the ab-

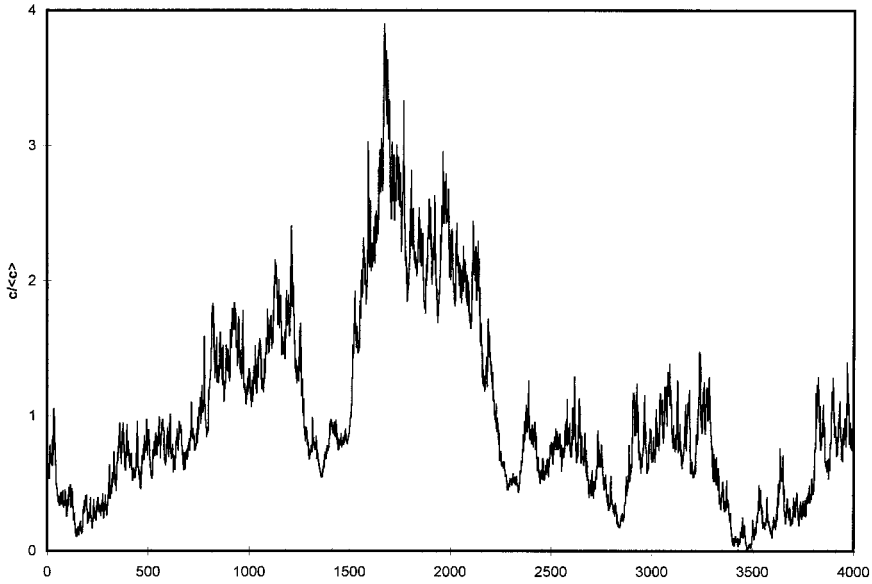

FIG. 5. Model data series for a well-mixed, homogeneous field ($\alpha = 1.7$, $C_1 = 0.10$, $H = 0.4$; see Table 1).

solute value of its differences between adjacent data points, that is, $\phi_{\Lambda,\mathrm{SF6}} = |\Delta\rho_{\mathrm{SF6}}|$. For the example 2-h case (Fig. 2) the (α, C_1) were (0.75, 0.315), (1.20, 0.16), and (1.42, 0.115) for the 50-, 100-, and 175-m towers, respectively (Fig. 4). The sensitivity of the estimates of α and C_1 for each case was examined individually with respect to moment order q and/or subrecord length within the scaling subrange. The variability in the estimate of C_1 for each case, typically about 0.01–0.02, exhibited greatest sensitivity to subrecord size A. The variability in α for each case was commonly in the range 0.01–0.03 and was sensitive to both moment order q and subrecord size. The variability in both parameters tended to increase as α decreased and C_1 increased.

The lowest values of α and largest values of C_1 were almost invariably associated with the 50-m tower. There was a tendency for the estimated α to increase and C_1 to decrease at towers farther downwind, especially at the 175- and 250-m towers. In fact, the α and C_1 values for the scalar SF_6 at 175 and 250 m approached values typical of those for other scalar fields in which homogeneous conditions are closely approximated (temperature and water vapor). Parameter values for SF_6 and other scalars from this study are compared with results from other field studies in Table 1. A brief summary of the meteorological conditions, relative position of the sensor within the plume, and multifractal parameter values for each case is shown in Table 2.

These results are consistent with the mixed multifractal nature of the measurements stemming from the line-source configuration of the experiment discussed above. The presence of zero gradients (i.e., consecutive zeros in the record) will affect the DTM analysis and estimates of α, an effect that increases toward the source as the number of zeros in the record increases. Measurements close to the line source are much more likely to be affected by the highly inhomogeneous margins of the plume or clean air incursions than farther downwind

TABLE 1. Summary of α, C_1, and H parameter values from different field studies. Asterisk (*) denotes results for more homogeneous plume conditions. Here T denotes temperature.

Reference	Passive scalar	Type	α	C_1	H
This paper	SF_6*	Time, atmosphere	1.60–1.80	0.095–0.12	0.4
This paper	H_2O	Time, atmosphere	1.60	0.07	—
Pelletier 1995	H_2O	Time, atmosphere	1.69	0.08	—
This paper	T	Time, atmosphere	1.69	0.09	0.44
Pelletier 1995	T	Time, atmosphere	1.69	0.08	—
Wang 1995	T	Time, atmosphere	1.69	0.10	0.41
Schmitt et al. 1996	T	Time, atmosphere	1.45	0.07	0.38
Seuront et al. 1999	T	Time, ocean	1.70	0.04	0.42
Chigirinskaya et al. 1994	T	Space, atmosphere	1.25	0.04	0.33
Lovejoy et al. 2000	T	Space, ocean	1.81	0.03	0.31
Average	All	Time	1.7	0.08 ± 0.02	0.41 ± 0.02

TABLE 2. Summary of meteorological and corresponding estimates of multifractal parameters. All column headings are described in text except for u_*, the friction velocity.

x	u_*	z/L	$dz/\bar{z}$	α	C_1	H	q_D
50	0.11	0.95	5.17	0.71	0.350		
50	0.20	0.43	3.46	0.50	0.430		
50	0.25	0.21	3.02	0.70	0.335		1.35
50	0.27	0.15	0.93	1.13	0.145	0.49	1.94
50	0.39	0.10	2.30	0.71	0.330		1.78
50	0.36	0.09	2.36	0.61	0.330		1.11
50	0.36	0.08	2.30	1.42	0.370	0.50	
50	0.45	0.06	2.25	0.94	0.315		
50	0.46	0.05	2.19	0.75	0.315		1.23
50	0.68	0.01	0.37	1.57	0.112	0.32	
50	0.37	−0.08	−0.06	1.16	0.140	0.37	
50	0.63	−0.12	1.31	1.35	0.225	0.39	
50	0.33	−0.13	−0.14	1.27	0.143	0.47	
50	0.44	−0.40	0.28	1.12	0.205	0.48	
50	0.39	−0.49	−0.18	1.18	0.230	0.50	1.78
100	0.11	0.95	3.40	0.98	0.210		
100	0.20	0.43	2.07	1.43	0.177	0.43	
100	0.25	0.21	1.64	1.16	0.160	0.42	1.61
100	0.27	0.15	0.33	1.34	0.120	0.50	1.16
100	0.39	0.10	1.15	1.30	0.150	0.51	1.44
100	0.36	0.09	1.15	1.24	0.145	0.37	1.58
100	0.36	0.08	1.06	1.28	0.165	0.44	
100	0.45	0.06	1.03	1.28	0.160	0.58	
100	0.46	0.05	0.99	1.20	0.160	0.44	1.30
100	0.68	0.01	−0.16	1.60	0.109	0.40	
100	0.37	−0.08	−0.51	1.43	0.110	0.41	
100	0.63	−0.11	0.20	1.13	0.155	0.37	
100	0.33	−0.12	−0.59	1.39	0.102	0.29	
100	0.39	−0.49	−0.68	1.06	0.128	0.35	1.41
175	0.11	0.95	2.36	1.05	0.165	0.43	
175	0.20	0.43	1.30	1.53	0.120	0.44	
175	0.25	0.21	0.93	1.36	0.124	0.38	1.32
175	0.27	0.15	−0.01	1.35	0.123	0.48	
175	0.39	0.10	0.49	1.45	0.110	0.42	2.13
175	0.36	0.09	0.49	1.52	0.114	0.39	2.97
175	0.36	0.08	0.45	1.65	0.110	0.44	
175	0.45	0.06	0.45	1.66	0.115	0.42	
175	0.46	0.05	0.36	1.42	0.115	0.46	1.88
175	0.68	0.01	−0.44	1.73	0.125	0.43	
175	0.37	−0.08	−0.74	1.40	0.120	0.41	
175	0.33	−0.12	−0.79	1.71	0.097	0.36	
175	0.63	−0.12	−0.33	1.32	0.110	0.34	
175	0.44	−0.40	−0.74	1.16	0.145	0.57	
175	0.39	−0.49	−0.87	1.20	0.127	0.43	2.03
250	0.11	0.95	1.89	1.45	0.140	0.24	
250	0.20	0.43	0.91	1.73	0.113	0.34	
250	0.25	0.21	0.59	1.46	0.110	0.33	1.35
250	0.27	0.15	−0.19	1.80	0.125	0.46	
250	0.39	0.10	0.20	1.59	0.110	0.39	1.85
250	0.36	0.09	0.21	1.55	0.119	0.53	
250	0.36	0.08	0.14	1.68	0.110	0.33	
250	0.45	0.06	0.11	1.64	0.110	0.46	
250	0.46	0.05	0.08	1.54	0.113	0.30	
250	0.68	0.01	−0.57	1.78	0.095	0.32	
250	0.37	−0.08	−0.83	1.80	0.115	0.38	
250	0.33	−0.12	−0.87	1.59	0.097	0.39	
250	0.63	−0.12	−0.55	1.58	0.115	0.40	
250	0.39	−0.49	−0.92	1.74	0.150	0.40	

where the effect of zeros diminishes. Low α and high C_1 are associated with the early, less-mature stages of scalar mixing. Increasing plume homogenization and spread of the plume by turbulent mixing for larger x (i.e., as $x \to \infty$, $c \to$ constant) is expressed by the shift in α to those valves more representative of a homogeneous, universal multifractal field ($\alpha \to \geq 1.6$).

c. Comparison of experimental and model results

The stochastic model was run for each case using the SF_6 experimental values of α, C_1, and H for α greater than 1. In general, any combination of decreasing H, decreasing α, and/or increasing C_1 will result in an increase in P/M or fluctuation intensity i_c for the stochastic model. The plume statistics from these nondimensional model time series were compared to the statistics for the corresponding 2-h experimental time series after the SF_6 concentrations had been averaged to 1 and 15 s. The former is close to the actual response characteristics of the analyzer, represents a likely minimum possible time span for any potential health consequences, and offers a comparison between the resolution of the internal plume structure by model and experimental data at high frequency. The latter tests the sensitivity of the model to longer averaging periods for P/M evaluation and is closer to a more probable duration for health effects. The ratios of the averaging time for the peak to the averaging time for the mean are about 1/7200 and 1/480 for 1 and 15 s, respectively.

The number of data points generated by the model was some power of 2 and was chosen to be similar in magnitude to the number of 1- or 15-s experimental data points for each 2-h period (e.g., 4096 or 8192 for 1-s averaging). Because the model is stochastic in nature, it was run 20 times for each (α, C_1, H) set from each case. The averages calculated from the 20 runs were used in the comparison between model and experimental results. For the experimental data, 1-s average values that were less than 1% of the maximum and varied by less than 1 ppt between adjacent points (i.e., approximately 0.01% of the maximum) were set equal to zero. This adjustment was done to minimize the effects of instrument noise in the presence of SF_6-free air. In a similar way, model points with values less than 1% of the maximum and fluctuations between adjacent points of less than 0.01% of the maximum were set equal to zero. For α less than 1.5, 11.6% and 20% of the model and experimental values were set to zero, respectively. For α greater than 1.5, 1.4% and 5.9% were set to zero. For the purpose of comparing the dimensional experimental quantities with the nondimensional model values, all values were normalized by their respective means. The stochastic model was run for each case using the experimental values of α, C_1, and H_{SF6} for α greater than 1.

The role of α as a key multifractal index and its ability to characterize multifractal signals, in this case the state of scalar mixing, suggests keying the analysis to α. A comparison between the 1-s experimental and model results for P/M as a function of α is shown on Fig. 6. For higher values of α, there is a tendency for the ex-

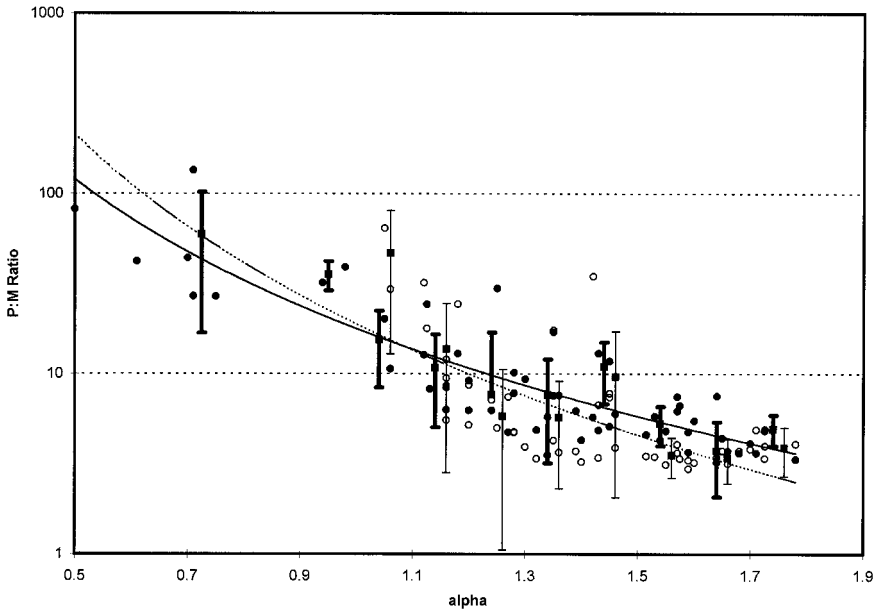

FIG. 6. Plot of 1-s average peak-to-mean ratios (P/M) from experimental measurements (●) and corresponding stochastic model results (○) vs α with uncertainty bars [measured (heavy lines), model (light lines); bin mean P/M (■)]. The trend lines, for emphasis only, are power-law fits to the P/M for experimental (solid) and model (dashed) points.

perimentally measured P/M to exceed the corresponding model result. For α from 1.0 to about 1.2 the modeled P/M ratios tend to be similar to or higher than the measured ratios. In all α bins ($\alpha > 1$), however, the uncertainty in the experimental value of P/M overlaps the uncertainty about the model value. Given the logarithmic axis, the uncertainty in P/M tends to increase for $\alpha \leq 1.2$.

The estimated values of α and C_1 as a function of the corresponding experimentally measured values of P/M and i_c for each 2-h case are shown in Figs. 7 and 8, respectively. Although a notable scatter exists, there is

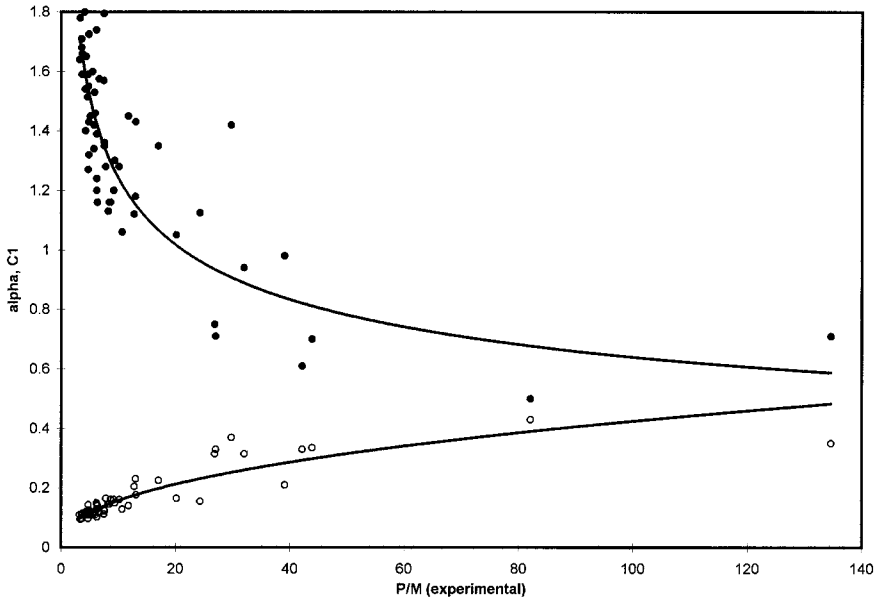

FIG. 7. Plot of α (●) and C_1 (○) values determined by DTM from SF_6 experimental data vs corresponding experimental values of peak-to-mean ratio (P/M). The trend lines are power-law fits, for emphasis only.

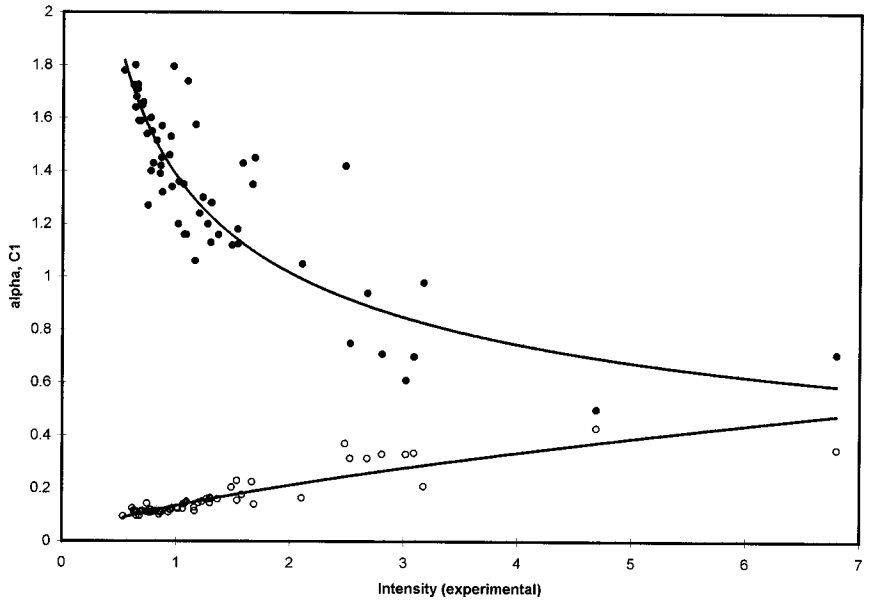

FIG. 8. Plot of α (●) and C_1 (○) values determined by DTM from SF_6 experimental data vs corresponding experimental values of fluctuation intensity i_c. The trend lines are power-law fits, for emphasis only.

an obvious suggestion of a correlation between these plume concentration characteristics and the corresponding α and C_1. This suggestion indicates that α and C_1 parameterize the state of mixing and turbulent concentration fluctuations. There is also a suggestion for a dependence of α and C_1 on the normalized distance from the mean plume height $\bar{z}$ to the measurement height, especially above z_m (Fig. 9). This result would reflect the influence of plume inhomogeneities near the margins. The value of the mean plume height $\bar{z}$ was found from the numerical solution of (van Ulden 1978)

$$\frac{d\bar{z}}{dx} = \frac{k^2}{[\ln(p\bar{z}/z_0) - \psi(p\bar{z}/L)]\phi_c(p\bar{z}/L)} \tag{6}$$

at each tower distance x for the experimentally determined values of L, where ψ is a surface layer similarity

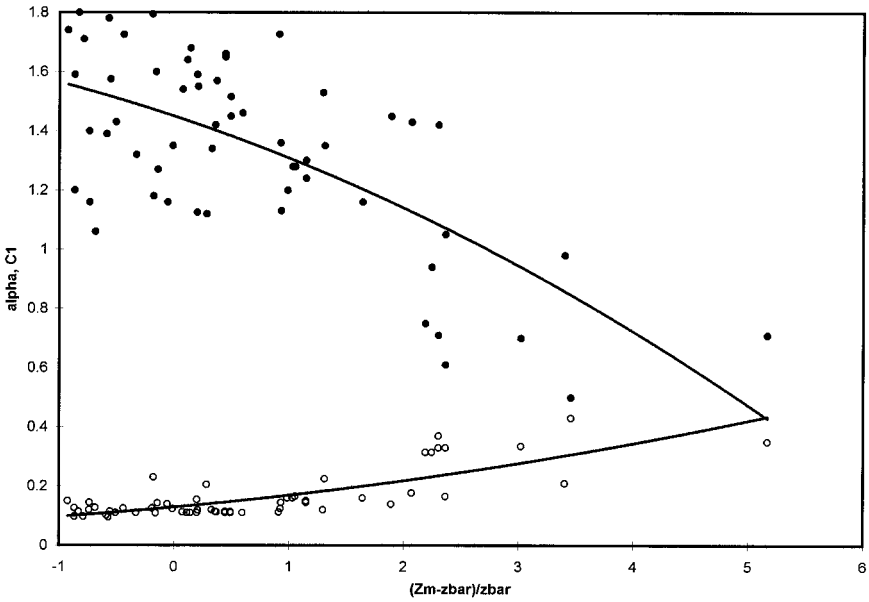

FIG. 9. Plot of α (●) and C_1 (○) values determined by DTM from SF_6 experimental data vs corresponding experimental values of the normalized distance from the mean plume height $\bar{z}$. The trend lines are power-law fits, for emphasis only.

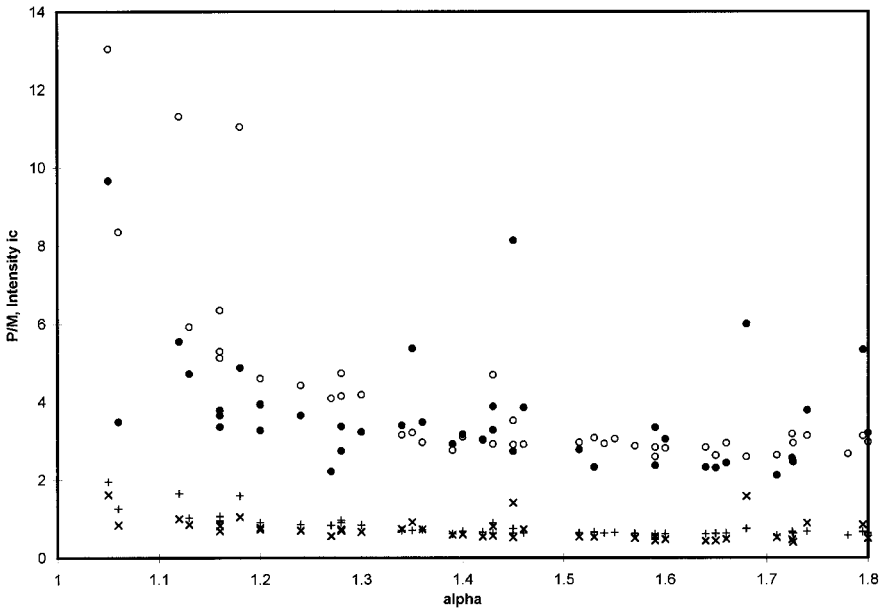

FIG. 10. Plot of 15-s average results for peak-to-mean ratio (P/M) (experimental ●; model ○) and fluctuation intensity i_c (experimental ×; model +) vs α.

correction for stability (Businger 1973), k is the von Kármán constant equal to approximately 0.40, and p is approximately 1.55. The dependence of α and C_1 on distance from the center of the plume is consistent with the inhomogeneous nature of the source and the presence of SF_6-free air aloft as discussed above.

A summary of the experimental and model results for the 15-s averaging time for P/M and i_c is shown in Fig. 10. These results suggest that the model can be used effectively at varying scales of resolution.

Figure 11 summarizes the comparison between experiment and model for P/M and i_c. The increase in the normalized mean-square error for P/M as α decreases can be explained in part by the much greater uncertainty in both the experimental and model estimates of P/M for small values of α.

The ability of the model to predict the probability of realizing a full spectrum of peak strengths rather than just P/M was then examined. The probability of the stochastic model predicting values at different multiples

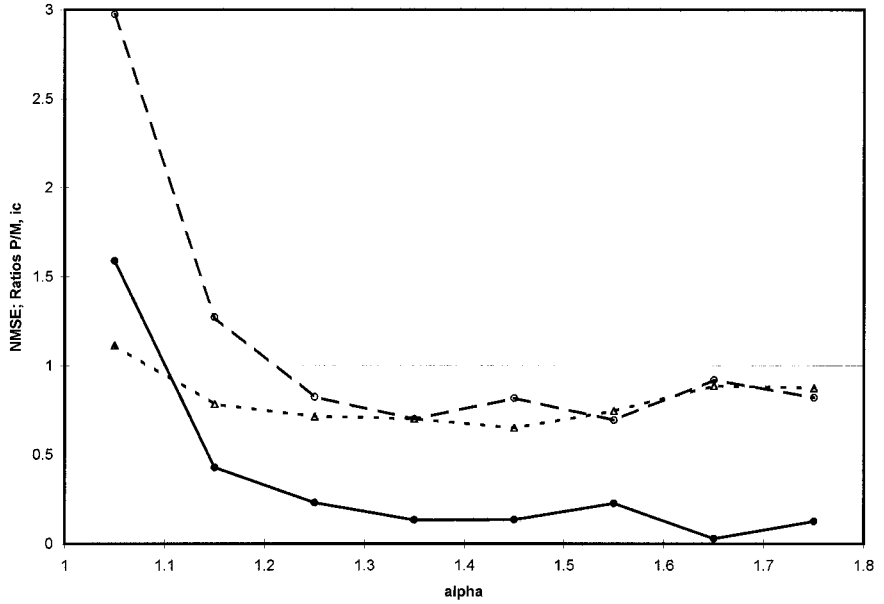

FIG. 11. Plot of the normalized mean-square error (●) and ratios of the mean model P/M:mean measured P/M (○) and mean model i_c:mean measured i_c (△) vs α.

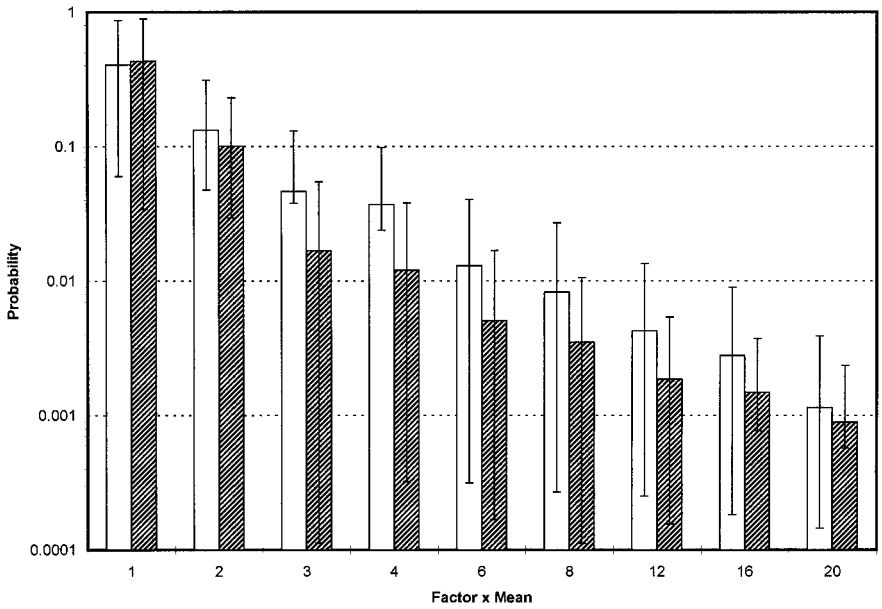

FIG. 12. Plot of the probability of experimental (clear) and model (patterned) estimates exceeding some multiple factor of their respective mean values.

of the mean value is compared with the observed probability of observing experimental values at different multiples of the mean (Fig. 12) (i.e., ''1'' = mean, ''2'' = 2 times the mean). This comparison is for the aggregate of all the experimental cases ($\alpha > 1$) and the corresponding model results using 1-s average values. The model predictions for the probability of realizing values at some multiple of the mean is generally less than, but always within an order of magnitude of, the observed experimental probabilities for all multiples of the mean.

d. Divergence of statistical moments, choice of q, and estimates of α and C_1

The scale dependency of actual measurements is a fundamental consequence of cascade processes concentrating conserved fluxes into smaller and smaller regions of space. However, the small-scale limit of such processes is singular, and a distinction must be made between ''bare'' and ''dressed'' cascade properties (Schertzer and Lovejoy 1987, 1991, 1993; Lavallee et al. 1993). A bare cascade is a theoretical cascade after a finite number of cascade steps ($\Lambda < \infty$). A dressed cascade, in contrast, is one that represents the spatially averaged, fully developed cascade ($\Lambda \to \infty$), integrated at the experimentally accessible scale of resolution of the measurement system.

Because the dressed cascade takes all the small-scale structure and interactions into account, it is more variable than the corresponding bare cascade. More precisely, the two will differ for all moments q greater than q_D when the dressed moments will diverge. This divergence has consequences for the choice of q in the estimation of α and C_1. Empirical moments for dressed (space/time block-averaged quantities) will diverge for moment orders q greater than or equal to a critical moment order q_D (Tr $\to \infty$ for $q > q_D$). The subscript D indicates that q_D is a function of the averaging space. Estimates of q_D can be obtained using the absolute value of the slope for the power-law scaling given by $\Pr(\Delta \mathrm{SF}_6 > y) \propto y^{-3q_D}$, where $\Delta \mathrm{SF}_6$ are the differences between adjacent data points, and y are thresholds. To obtain the best statistics, data at the highest available resolution are used (Chigirinskaya et al. 1994; Schmitt et al. 1994).

Examples of this analysis for SF_6 are shown in Fig. 13 with results of selected cases reported in Table 2. The mean $q_{D,\mathrm{SF6}}$ for the SF_6 scalar is 1.58. This mean value is less than the values for horizontal wind velocity found in this study ($q_{D,u} \approx 2.43$). The low values for $q_{D,\mathrm{SF6}}$ and its large variability are consistent with the inhomogeneity of the SF_6 fields. The choice of a low value of q ($q = 0.8$) for estimation of α and C_1 was made out of consideration for the low values of $q_{D,\mathrm{SF6}}$.

Theoretically $K(q, \eta)$ is a convex function. However, empirical datasets are finite, and sufficiently high-order moments cannot be accurately estimated. In particular, the scaling will become spurious [$K(q, \eta)$ becomes linear], diverging for $q\eta > q_D$ or $\eta > q_D$, and the use of Eq. (3) breaks down. This breakdown will occur whenever $\max(q, q\eta) \geq \min(q_s, q_D)$ where q_s is the maximum moment that can be estimated using a finite number of N independent samples and is given by $q_s = [(D + D_s)/C_1]^{1/\alpha}$. The sampling dimension D_s equals $\log N/\log\lambda$, and $D = 1$ for a one-dimensional time series (Schertzer and Lovejoy 1989). The constraint by q_s can be overcome by increasing the sampling, whereas the constraint

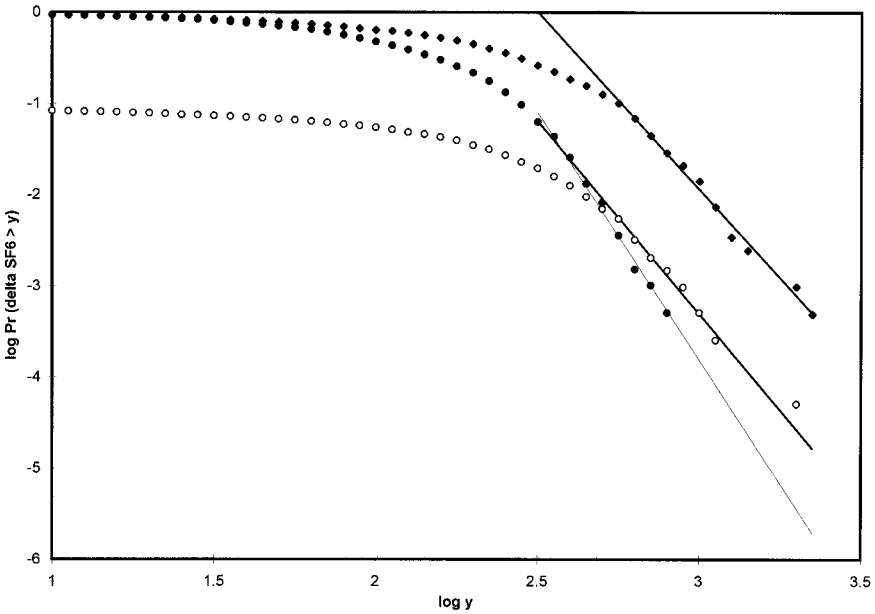

FIG. 13. Plot of $\Pr(\Delta SF_6 > y) \sim y^{-3qD}$ for selected cases [(♦) 100-m tower, yeardays 173 to 174, 2300–0100 local time, $q_{D,SF6} = 1.30$; (○) 100-m tower, yearday 168, 1100–1300 local time, $q_{D,SF6} = 1.41$; (●) 175-m tower, yeardays 173 to 174, 2300–0100 local time, $q_{D,SF6} = 1.81$]. The lines are slopes used for estimating q_D.

by q_D is a fundamental limitation related to averaging to the highest available resolution, which may be much larger than the actual inner scale of homogeneity (e.g., the physical limit of viscous dissipation).

5. Discussion

It is clear that the plume parameters P/M and i_c are sensitive to the values of α and C_1 and that the determination of α and C_1 is a function of the state of mixing and the magnitude of the variability in the signal. The α and C_1 for SF_6 from the line source approach values representative of passive scalars from homogeneous sources as the zeros disappear and plume homogeneity increases downwind.

The indication of a relationship between (α, C_1) and P/M raises the prospect of using the codimension multifractal methodology for the analysis and prediction of large-magnitude events that greatly exceed the mean. The method is capable of describing the inherently large variability in plume concentrations. Once the parameters α, C_1, and H have been established for a given situation, it would be an easy matter to model the process at other timescales of resolution. The greatest obstacles to its use are the need to obtain suitable quality datasets for parameter estimation with regard to the presence of scaling, data size, measurement resolution and accuracy, and the uncertainties associated with its use, especially for small values of α or large values of C_1. In this respect, it is pointed out that the stochastic prediction of P/M is sensitive to the selected record length. On the other hand, one of the utilities of the stochastic model is the ability to make estimates of the probability of realizing extreme events at timescales of observation beyond or at magnitudes in excess of those present in the actual observations. This estimation can be accomplished by using the model to generate arbitrarily long data series. An alternate multifractal method of evaluating extreme events is with use of the maximum sampling singularity γ_s (e.g., Pandey et al. 1998).

The methodology has potential applications to a wide variety of natural geophysical processes whose measured signals are commonly multifractal in character. Among the possibilities implicated by this research is application of the methodology to the modeling of point-source plumes. Assuming it can be linked to a model describing point-source plume meander, the multifractal methodology can be used for analyzing concentration fluctuations within plumes. Within the plume, scalar time series from a line source can mimic those from a point source. Plumes of any origin can exhibit sharp variations in concentration above and about the mean as measured by P/M and i_c, respectively. The state of mixing within line-source and point-source plumes will be similar near the source, near the margins, or farther downwind after extensive mixing. It is conjectured that the multifractal results for line- and point-source plumes would be similar with respect to these controls. It was beyond the scope of this study, but it might be possible to generate dimensional concentration data series by calibrating model results against the measured experimental data from which the multifractal parameters were determined (e.g., set the mean of the model data series equal to the mean of the experimental data series and

scale the model data series accordingly). Alternately, they might be calibrated against the mean concentrations predicted by other kinds of models.

One of the constraints on this analysis was the limited scaling ranges of the SF_6 power spectra. This introduced uncertainty into several aspects of the analysis. First, it increased the uncertainty in the determination of β from the slope of the spectra. Second, it led to some uncertainty in the identification of the optimum scaling range for use in determining the α and C_1 parameters. A closely related point is how the shortened scaling ranges restricted the subrecord lengths that could be used for finding the multifractal parameters. Ideally, the longest possible subrecord A should be used to minimize the uncertainties involved with the estimates of α and C_1. Provided a sufficient scaling range is present, however, the DTM algorithm can be used.

6. Conclusions

The use of the DTM technique for the analysis and description of the plume concentration characteristics P/M and i_c for a line source has been demonstrated. The multifractal parameters α and C_1 express the state of mixing, and there is a definite correspondence between α and C_1 and the measured P/M and i_c. Furthermore, it is possible to use the results of experimental measurements, the DTM technique, and a stochastic multifractal model to analyze and to predict in-plume concentration fluctuations and the state of scalar mixing. There are significant uncertainties associated with use of the multifractal model, but the uncertainties in the model results overlapped the uncertainties in the measurements in every case. The large uncertainties are a direct reflection of the large natural variability exhibited by plumes.

Acknowledgments. This research was funded in part by the National Science Foundation under Grant ATM-9016537. We acknowledge the assistance of Y. Wang and Y. Tessier. Individuals who contributed to the realization of the experiment include T. Horst, G. Maclean, T. Delany, S. Semmer, and other ASTER division personnel from the National Center for Atmospheric Research; J. Allwine from Pacific Northwest Laboratories; and L. Bamesberger, J. Rydock, and B. Siverson of Washington State University.

APPENDIX

Summary of Multifractal Theory

The multifractal model of turbulence is a consequence of the intermittency basis of the cascade theory for the inertial subrange (Richardson 1922; Yaglom 1966; Novikov and Stewart 1964; Mandelbrot 1974; Sreenivasan 1991; Schertzer and Lovejoy 1987, 1989; Monin and Yaglom 1975); this implies that power-law scaling is present in the observed process. In brief, cascade theory states that energy or other conserved flux will be conserved, on average, but nonuniformly redistributed as it passes from larger scales to smaller scales. This results in the flux, on each realization, being concentrated into smaller regions of space and the creation of steep gradients, intermittency, and a multifractal field.

A fractal is a scale-invariant geometric set of points, and a multifractal is a scale-invariant field; the set of points exceeding any specified signal magnitude (threshold) is a fractal set whose dimension depends on the threshold used to define it. A (mono)fractal field is distinguished from a multifractal field by the fact that it is independent of any threshold, that is, the signal is either ''off'' or ''on.'' A concentration field is multifractal because a different set of points and filling of the available geometric measurement space will be defined as the threshold changes. As the threshold increases, fewer and fewer points will be included in the fractal set corresponding to each threshold.

Multifractal fields have traditionally been studied using monofractal box-counting techniques based on the geometric dimension of the measurement space. This ''functional box-counting'' approach (Lovejoy et al. 1987) quantifies the filling of the embedding space by a concentration measurement as a function of resolution. The application of box-counting techniques to multifractals is achieved by assuming the fractal dimensions are dependent on scalar concentration and then systematically varying the concentration threshold. In this geometric dimension approach, $D_f + C_f = D$, where D_f is the fractal dimension and quantifies the filling of space, C_f is the codimension, and D is the geometric dimension of the embedding space of the time or space series measurement. This geometric approach is constrained to the analysis of signals where D_f is less than D and C_f is less than D. When C_f is greater than D, however, the result is a negative fractal dimension and the ''latent paradox'' (Mandelbrot 1989).

In contrast, the statistical codimension multifractal formalism (Schertzer and Lovejoy 1987, 1989) avoids this problem because the codimension is defined in an infinite dimensional probability space and is independent of the embedding dimension. In this approach, the codimension quantifies the relative filling of the total probability space and C_f can exceed D. An implementation of this approach is described in the main text.

The codimension function $c(\gamma)$ characterizing the statistics of the conserved multifractal measure density μ (nondimensionalized by the mean) is defined by

$$\Pr(\phi_\lambda \geq \lambda^\gamma) \approx \lambda^{-c(\gamma)}, \tag{A1}$$

where Pr is probability. The symbol λ denotes the scale of resolution of the measurement. The symbol γ denotes the singularity magnitude ($\approx \log\phi_\lambda/\log\lambda$). The ''$\approx$'' sign denotes equality to within slowly varying factors. The λ^γ notation specifies a threshold level. The function $c(\gamma)$, then, is the scaling exponent of the probability distributions of the conserved measure density ϕ at ar-

bitrary resolutions λ. The probability that the signal will be observed will decrease as the threshold λ^{γ} increases, that is, fewer peaks will reach above the threshold. Knowledge of the statistical moments, $K(q, \eta)$, is generally equivalent to knowledge of the probability distributions and is convenient for statistical analysis.

A conserved signal refers to a time or space series in which the mean is equivalent at all time/space scales of observation. It is the direct result of a multiplicative cascade process in which the quantity is conserved from one scale to the next in the cascade. Therefore, it is independent of the scale of resolution λ. Recall that the sum of the spectral power over all frequencies is the variance. In classical theory of turbulence there are two conserved fluxes from the large scale to the dissipation scale, the energy flux ε and the passive scalar variance flux χ, both which are proportional to variance. The fluxes ε and χ are conserved by the nonlinear equations: $\langle \varepsilon_\lambda \rangle$ = constant and $\langle \chi_\lambda \rangle$ = constant where "$\langle\ \rangle$" denotes the ensemble mean. By essentially dimensional arguments, the observed velocity shears Δv_λ and scalar concentration fluctuations $\Delta \rho_\lambda$ are related by $\Delta v_\lambda = \varepsilon_\lambda^{1/3} \lambda^{-1/3}$ and $\Delta \rho_\lambda = \phi_\lambda^{1/3} \lambda^{-1/3}$ (Corrsin 1951; Obukhov 1949), where $\phi_\lambda = \chi_\lambda^{3/2} \varepsilon_\lambda^{-1/2}$. The scaling factor of the form λ^{-H} is necessary for satisfying the requirement that ϕ must be conserved from one scale to the next.

The quantity used in analyzing a multifractal cascade process must be conserved from one scale to the next. In general, however, an observed data series ρ is not conserved and must be transformed into a conserved signal, generically denoted ϕ, using the scaling factor of the form λ^{-H}. From the above, the measured time series signal ρ is generically related to the conserved signal ϕ by some scale-changing operation involving only the dimensionless scale of resolution λ (Schertzer and Lovejoy 1987, 1993; Lavallee et al. 1993; Schmitt et al. 1992):

$$\rho_\lambda = \phi_\lambda \lambda^{-H}. \tag{A2}$$

The parameter H is one of three universal multifractal parameters and characterizes the degree of nonconservation. A conserved flux can be obtained from a nonconserved signal by fractional differentiation of ρ by an order H (e.g., power-law filtering in Fourier space). This represents the transformation of observations made at some scale of resolution into a conserved quantity that is proportional to variance. For conserved multifractals, H is equal to 0 and is ⅓ for ε and χ in Eq. (A2).

REFERENCES

Benner, R. L., and B. Lamb, 1985: A fast response continuous analyzer for halogenated atmospheric tracers. *J. Atmos. Oceanic Technol.,* **2,** 582–589.

Businger, J., 1973: Turbulent transfer in the atmospheric surface layer. *Workshop on Micrometeorology,* D. A. Haugen, Ed., Amer. Meteor. Soc., 67–100.

Chigirinskaya, Y., D. Schertzer, S. Lovejoy, A. Lazarev, and A. Ordanovich, 1994: Unified multifractal atmospheric dynamics tested in the tropics: Part I, horizontal scaling and self-criticality. *Nonlinear Proc. Geophys.,* **1,** 105–114.

Constantin, P., I. Procacia, and K. R. Sreenivasan, 1991: Fractal geometry of isoscalar surfaces in turbulence: Theory and experiments. *Phys. Rev. Lett.,* **67,** 1739–1742.

Corrsin, S., 1951: On the spectrum of isotropic temperature fluctuations in an isotropic turbulence. *J. Appl. Phys.,* **22,** 469–473.

Feller, W., 1971: *An Introduction to Probability Theory and its Applications.* Vol. 2. John Wiley and Sons, 669 pp.

Finn, D. F., B. Lamb, M. Y. Leclerc, and T. W. Horst, 1996: Experimental evaluation of analytical and Lagrangian surface layer flux footprint models. *Bound.-Layer Meteor.,* **80,** 283–308.

Hanna, S. R., 1984: The exponential probability density function and concentration fluctuations in smoke plumes. *Bound.-Layer Meteor.,* **29,** 361–375.

——, and E. M. Insley, 1989: Time series analysis of concentration and wind fluctuations. *Bound.-Layer Meteor.* **47,** 131–147.

Kaimal, J. C., J. C. Wyngaard, Y. Izumi, and O. R. Cote, 1972: Spectral characteristics of surface-layer turbulence. *Quart. J. Roy. Meteor. Soc.,* **98,** 563–589.

Larsen, S. E., and S.-E. Gryning, 1986: Dispersion climatology in a coastal zone. *Atmos. Environ.,* **20,** 825–856.

Lavallee, D., S. Lovejoy, D. Schertzer, and P. Ladoy, 1993: Nonlinear variability of landscape topography: Multifractal analysis and simulation. *Fractals in Geography,* L. D. Cola and N. Lam, Eds., Prentice-Hall, 171–205.

Lovejoy, S., D. Schertzer, and A. A. Tsonis, 1987: Functional box-counting and multiple dimensions in rain. *Science,* **235,** 1036–1038.

——, Y. Tessier, M. R. Claereboudt, W. J. S. Currie, J. C. Roff, E. Bourget, and D. Schertzer, 2000: Universal multifractals and ocean patchiness: Phytoplankton, physical fields and coastal heterogeneity. *J. Plankton Res.,* in press.

Malinowski, S., and M. Y. Leclerc, 1994: Fractal properties of temperature fluctuations in the convective surface layer. *Bound.-Layer Meteor.,* **71,** 169–187.

Mandelbrot, B., 1974: Intermittent turbulence in self-similar cascades: Divergence of high moments and dimension of the carrier. *J. Fluid Mech.,* **62,** 331–350.

——, 1989: Multifractal measures, especially for the geophysicist. *Pageoph.,* **131,** 5–42.

Mikkelsen, T., S. E. Larsen, and H. L. Pecseli, 1987: Diffusion of Gaussian puffs. *Quart. J. Roy. Meteor. Soc.,* **113,** 81–105.

Monin, A. S., and A. M. Yaglom, 1975: *Statistical Fluid Mechanics: Mechanics of Turbulence.* Vol. 2. MIT Press, 874 pp.

Muzzio, P. J., C. Meneveau, P. D. Swanson, and J. M. Ottino, 1992: Scaling and multifractal properties of mixing in chaotic flows. *Phys. Fluids A,* **4,** 1439–1456.

Novikov, E. A., and R. Stewart, 1964: Intermittency of turbulence and spectrum of fluctuations in energy-dissipation. *Izv. Akad. Nauk. SSSR Ser. Geofiz.,* **3,** 408–412.

Obukhov, A., 1949: Structure of the temperature field in a turbulent flow. *Izv. Akad. Nauk. SSSR Ser. Geogr. Geofiz.,* **13,** 55–69.

Pandey, G., S. Lovejoy, and D. Schertzer, 1998: Multifractal analysis of daily river flows including extremes for basins of five to two million square kilometers, one day to 75 years. *J. Hydrol.,* **208,** 62–81.

Pecknold, S., S. Lovejoy, D. Schertzer, C. Hooge, and J. F. Malouin, 1993: The simulation of universal multifractals. *Cellular Automata: Prospects in Astronomy and Geophysics,* J. M. Perdgang and A. Lejeune, Eds., World Scientific, 228–267.

Pelletier, R., 1995: Multifractal characterization of aircraft-based measurements of turbulence and passive scalar fields within the surface boundary layer. M.S. thesis, Dept. of Natural Resource Sciences, McGill University, 93 pp. [Available from Dept. of Natural Resource Sciences, McGill University, 845 Sherbrooke St. W., Montreal, PQ H3A 2T5 Canada.]

Peterson, H., and B. Lamb, 1992: Comparison of results from a meandering-plume model with measured atmospheric tracer concentration fluctuations. *J. Appl. Meteor.,* **31,** 553–564.

——, and ——, 1995: An investigation of instantaneous diffusion and concentration fluctuations. *J. Appl. Meteor.*, **34,** 2724–2746.

——, ——, and D. Stock, 1990: Interpretations of measured tracer concentration fluctuations using a sinusoidal meandering plume model. *J. Appl. Meteor.*, **29,** 1284–1299.

——, P. Ballard, and B. Lamb, 1995: A new Lagrangian approach to studying instantaneous plume dispersion and concentration fluctuations. Preprints, *11th Symp. on Boundary Layers and Turbulence*, Charlotte, NC, Amer. Meteor. Soc., 140–143.

Praskovsky, A. A., W. F. Dabberdt, and E. A. Praskovsky, 1996: Fractal geometry of isoconcentration surfaces in a smoke plume. *J. Atmos. Sci.*, **53,** 5–21.

Ramsdell, J. V., and W. T. Hinds, 1971: Concentration fluctuations and peak-to-mean ratios in plumes from a ground-level continuous point source. *Atmos. Environ.*, **5,** 483–495.

Richardson, L. F., 1922: *Weather Prediction by Numerical Processes.* Cambridge University Press. (Reprint, Dover, 1965.)

Salvadori, G., S. P. Ratti, G. Belli, S. Lovejoy, and D. Schertzer, 1994: Multifractal objective analysis of Seveso ground pollution. *J. Toxicol. Environ. Chem.*, **43,** 63–76.

Sawford, B. L., 1985: Lagrangian statistical simulation of concentration mean and fluctuation fields. *J. Climate Appl. Meteor.*, **24,** 1152–1166.

——, and H. Stapountzis, 1986: Concentration fluctuations according to fluctuating plume models in one and two dimensions. *Bound.-Layer Meteor.*, **37,** 89–105.

Schertzer, D., and S. Lovejoy, 1987: Physical modeling and analysis of rain clouds by anisotropic scaling multiplicative processes. *J. Geophys. Res.*, **92,** 9693–9714.

——, and ——, 1989: Generalized scale invariance and multiplicative processes in the atmosphere. *Pageoph.*, **130,** 57–81.

——, and ——, 1991: Nonlinear geodynamical variability: Multiple singularities, universality and observables. *Non-Linear Variability in Geophysics*, D. Schertzer and S. Lovejoy, Eds., Kluwer Academic, 41–82.

——, and ——, 1993: Nonlinear variability in geophysics 3; Scaling and multifractal processes. *Lecture Notes from AGU Chapman/EGS Richardson Memorial Conf.*, Cargese, France, 292 pp.

——, and ——, 1997: Universal multifractals do exist!: Comments on ''A statistical analysis of mesoscale rainfall as a random cascade.'' *J. Appl. Meteor.*, **36,** 1296–1303.

——, ——, and F. Schmitt, 1995: Structures in turbulence and multifractal universality. *Small-Scale Structures in Three-Dimensional Hydro and Magnetohydrodynamic Turbulence*, M. Meneguzzi, A. Pouquet, and P. L. Sulem, Eds., *Lecture Notes in Physics*, Vol. 462, Springer-Verlag, 137–144.

Schmitt, F., D. Lavallee, D. Schertzer, and S. Lovejoy, 1992: Empirical determination of universal multifractal exponents in turbulent velocity fields. *Phys. Rev. Lett.*, **68,** 305–308.

——, D. Schertzer, S. Lovejoy, and Y. Brunet, 1993: Estimation of universal multifractal indices for atmospheric turbulent velocity fields. *Fractals*, **1,** 568–575.

——, ——, ——, and ——, 1994: Empirical study of multifractal phase transitions in atmospheric turbulence. *Nonlinear Proc. Geophys.*, **1,** 95–104.

——, S. Lovejoy, and D. Schertzer, 1995: Multifractal analysis of the Greenland ice-core project climate data. *Geophys. Res. Lett.*, **22,** 1689–1692.

——, ——, ——, and Y. Brunet, 1996: Multifractal temperature and flux of temperature variance in fully developed turbulence. *Europhys. Lett.*, **34,** 195–200.

Seuront, L., F. Schmitt, Y. Lagadeuc, D. Schertzer, and S. Lovejoy, 1999: Universal multifractal analysis as a tool to characterize multiscale intermittent patterns: Example of phytoplankton distribution in turbulent coastal waters. *J. Plankton Res.*, **21,** 877–922.

Shen, S., and M. Y. Leclerc, 1994: Large eddy simulation of small-scale effects on the convective boundary layer structure. *Atmos.–Ocean.*, **32,** 717–730.

Sreenivasen, K. R., 1991: Fractals and multifractals in fluid turbulence. *Ann. Rev. Fluid Mech.*, **23,** 539–600.

——, R. Ramshankar, and C. Meneveau, 1989: Mixing, entrainment and fractal dimension of surfaces in turbulent flows. *Proc. Roy. Soc. London A,* **421,** 79–103.

Stapountzis, H., B. L. Sawford, J. C. R. Hunt, and R. E. Britter, 1986: Structure of the temperature field downwind of a line source in grid turbulence. *J. Fluid Mech.*, **165,** 401–424.

Sykes, R. I., R. S. Gabruk, and D. S. Henn, 1995: A multifractal representation of the small-scale structure in a turbulent plume. *J. Appl. Meteor.*, **34,** 2294–2305.

Tchiguirinskaia, I., S. Lu, F. J. Molz, T. M. Williams, and D. Lavallee, 2000: Multifractal versus monofractal analysis of wetland topography. *Stochastic Environ. Res. Risk Assess.*, **14,** 8–32.

Tessier, Y., S. Lovejoy, and D. Schertzer, 1994: Multifractal analysis and simulation of the global meteorological network. *J. Appl. Meteor.*, **33,** 1572–1586.

van Ulden, A. P., 1978: Simple estimates for vertical diffusion from sources near the ground. *Atmos. Environ.*, **12,** 2125–2129.

Wang, Y., 1995: Measurements and multifractal analysis of turbulent temperature and velocity near the ground. M. S. thesis, Dept of Natural Resource Sciences, McGill University, 84 pp. [Available from Dept. of Natural Resource Sciences, McGill University, 845 Sherbrooke St. W., Montreal, PQ H3A 2T5 Canada.]

Wilson, J., D. Schertzer, and S. Lovejoy, 1991: Continuous multiplicative cascade models of rain and clouds. *Non-Linear Variability in Geophysics*, D. Schertzer and S. Lovejoy, Eds., Kluwer Academic, 185–207.

Yaglom, A. M., 1966: The influence on the fluctuation in energy dissipation on the shape of turbulent characteristics in the inertial interval. *Sov. Phys. Dokl.*, **2,** 26–30.

Yee, E., P. R. Kosteniuk, G. M. Chandler, C. A. Biltoft, and J. F. Bowers, 1993: Statistical characteristics of concentrations fluctuations in dispersing plumes in the atmosphere surface layer. *Bound.-Layer Meteor.*, **65,** 69–109.

——, R. Chan, P. R. Kosteniuk, G. M. Chandler, C. A. Biltoft, and J. F. Bowers, 1994: Experimental measurements of concentration fluctuations and scales in a dispersing plume in the atmospheric surface layer obtained using a very fast response concentration detector. *J. Appl. Meteor.*, **33,** 996–1016.